Electronic Supplementary Material (ESI) for RSC Advances

Interplay of formation kinetics for highly oriented and mesostructured silicate-surfactant films at air-water interface

Ying-Huang Lai,[*,†,‡] *Siang-Wei Cheng,*[‡] *Shiaw-Woei Chen,*[‡] *Je-Wei Chang,*[‡] *Chun-Jen Su,*[†] *An-Chung Su,*[⊥] *Hwo-Shuenn Sheu,*[†] *Chung-Yuan Mou,*[∥] *U-Ser Jeng,*[*,†,⊥]

[†] National Synchrotron Radiation Research Center, Hsinchu Science Park, Hsinchu 30076, Taiwan

[‡] Department of Chemistry, Tunghai University, Taichung 407, Taiwan

[⊥] Department of Chemical Engineering, National Tsing Hua University, Hsinchu 30013, Taiwan

[∥] Department of Chemistry and Center of Condensed Matter Science, National Taiwan University, Taipei 106, Taiwan

[*] E-mail: yhlai@thu.edu.tw; usjeng@nsrrc.org.tw

1. TEM result of a mesostructured Si-CTAB film formed at the air-water interface

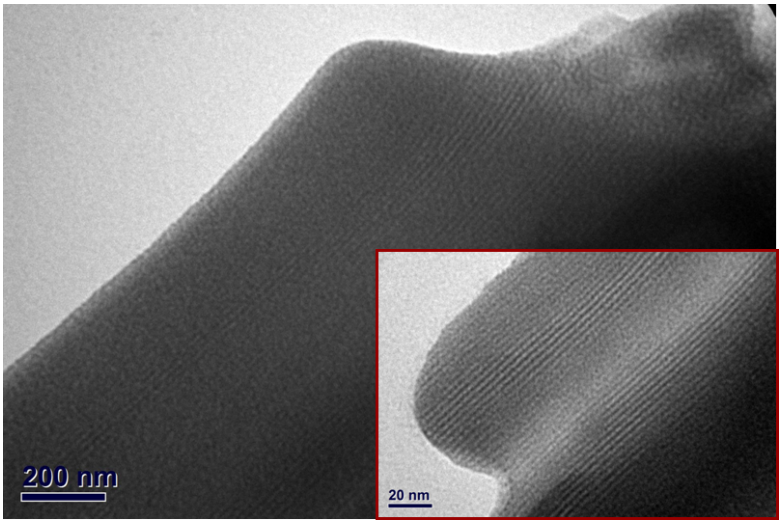

Figure S1. A represented TEM image and a room-in view (inset) for a mesostructured Si-CTAB film harvested from the air-water interface, showing the well-aligned channel structure.

2. CTAB micelles in solution and Si-CTAB micelles at the air-water interface

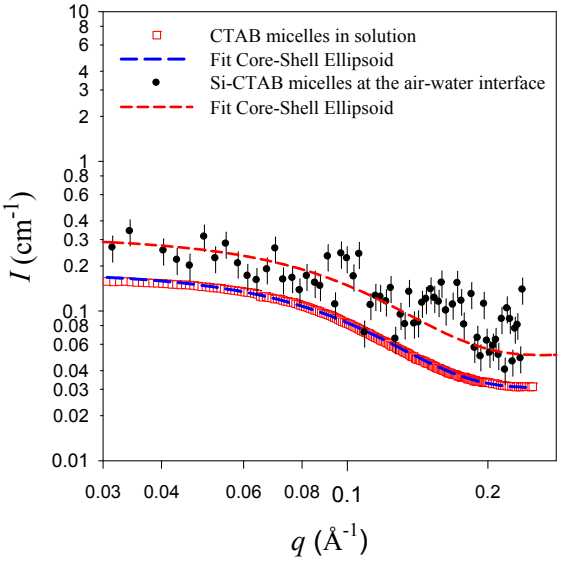

Figure S2. SAXS data for the CTAB solution in the absence of TEOS are fitted (long-dashed curve) using a model of core-shell prolate ellipsoids with semi-major and semi-minor axes of A = 33.0 Å and B =17.8 Å, along with shell thickness (headgroup region) σ = 2.0 Å. The first nontrivial set of GISAXS data at $t \approx 1300$ s (cf. Figure 1) are fitted (short-dashed curve) using the same model, with resembling parameters of A = 33.1 Å, B =17.7 Å, and σ = 2.5 Å.

3. Silicate concentration effect

Shown in Figure S2 are the phase evolutions of the mesostructure silicate-CTAB films observed at the air-water interface, at 25 °C, for the standard solution (at TEOS concentration C_T) and solutions with four-times (i.e., $4C_T$) or one-fourth (i.e., $C_T/4$) of the standard TEOS content. With decreasing silicate concentration from $4C_T$ to $C_T/4$, the induction time was significantly lengthened from 60 to 9000 s, respectively. Nevertheless, the same L-to-H kinetic pathway is followed in all three cases, as illustrated in Figure S2.

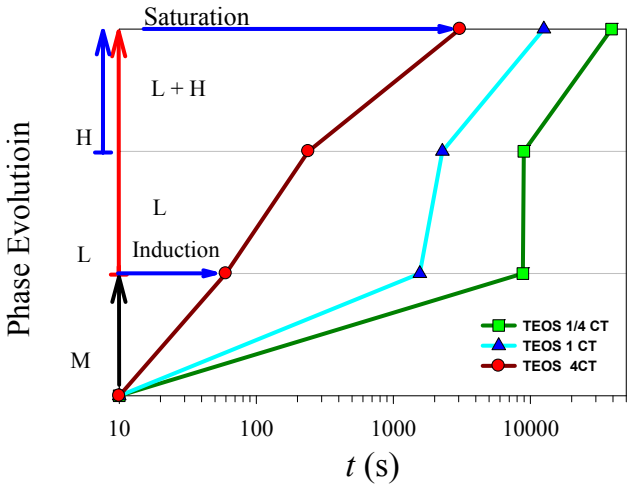

Figure S3. Phase evolution of the three solutions with different TEOS concentrations ($4C_T$, C_T, and $C_T/4$) all followed the same kinetic pathway of isotropic micelles (M) to lamellar (L) phase, and then quantitative transformation of L domains to 2D hexagonal (H) phase.

4. Acidity effects on Si-CTAB micelles

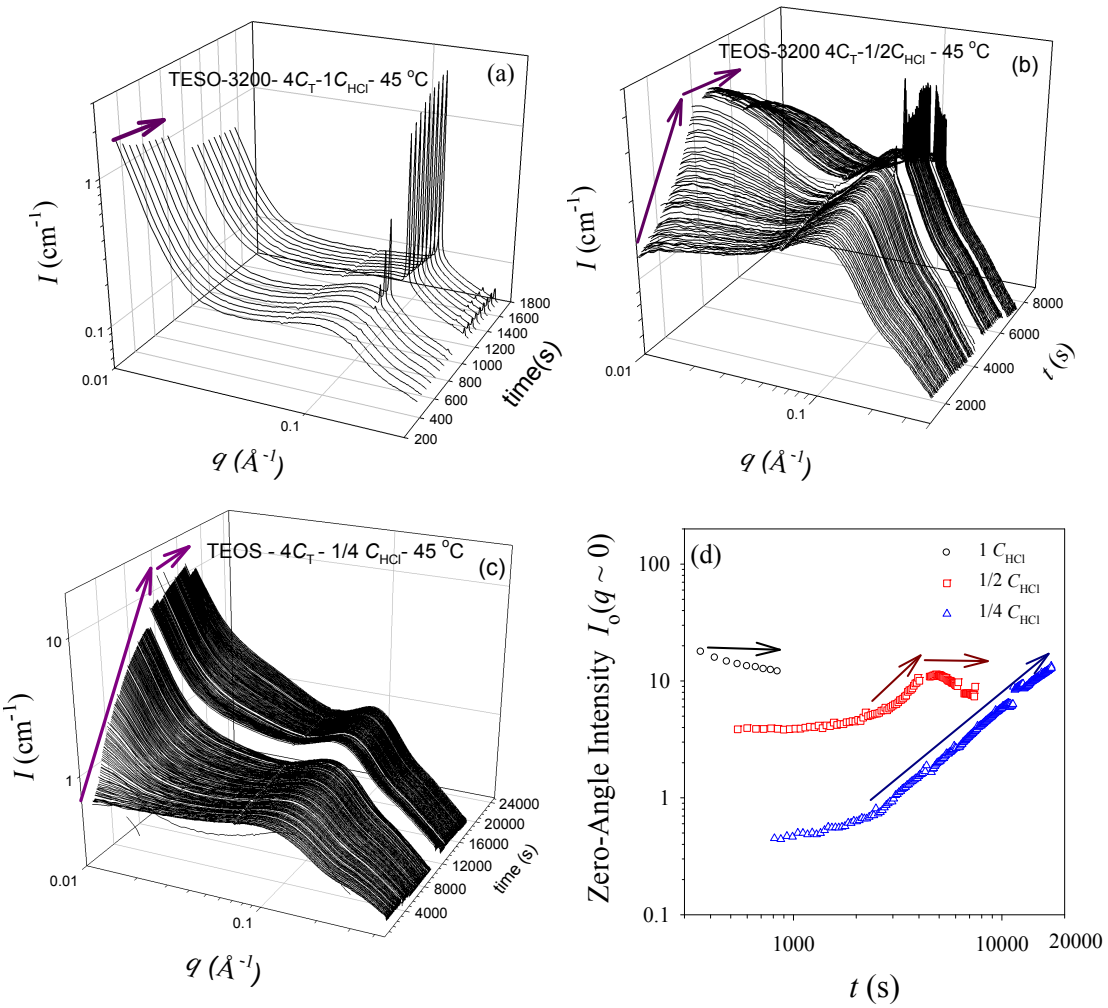

Figure S4: Time-resolved SAXS data measured at 45 °C for (a) a solution of silicate concentrations $4C_T$ and for similar solutions with decreased acid concentrations of (b) $C_{HCl}/2$ and (c) $C_{HCl}/4$. Thick arrows indicate the increasingly slower development of the "zero-angle" intensity I_o (at $q \approx 0.01$ Å^{-1}) with decreasing acidic level. (d) Corresponding evolutions of I_o. Note the extremely lengthened growth time for the solution of $C_{HCl}/4$.

5. In-situ SAXS data for silicate-CTAB sample solutions sealed without the air-water interface

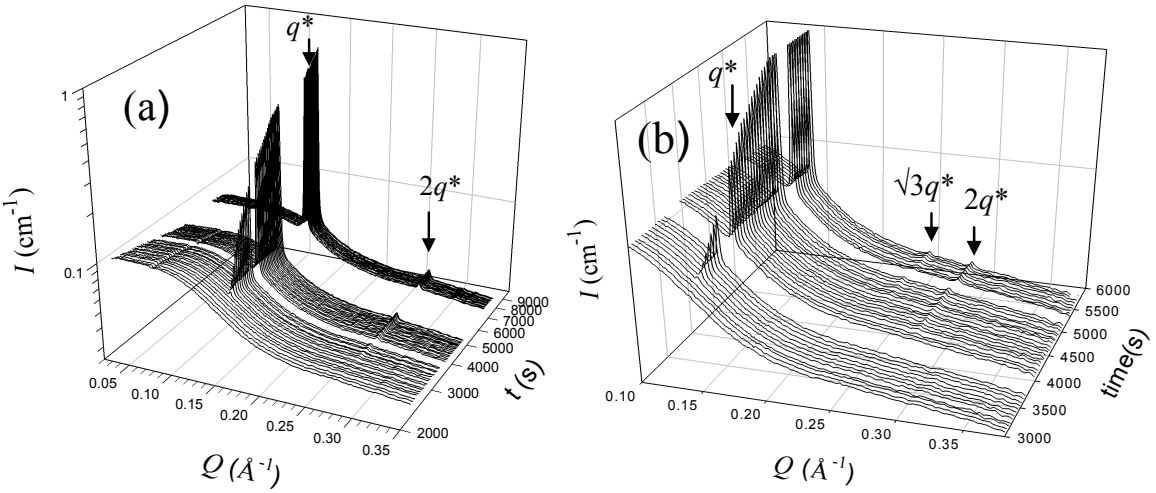

Figure S5: In-situ SAXS data measured for sealed solutions (of the reference sample composition) devoid of an air-water interface, displaying (a) L peaks at q^* and $2q^*$ at 25 °C and (b) H peaks at q^*, $3^{½}q^*$, and $2q^*$ at 45 °C.